ADVANCED FUNCTIONAL MATERIALS
www.afm-journal.de

Mesoporous $NiCo_2O_4$ Nanowire Arrays Grown on Carbon Textiles as Binder-Free Flexible Electrodes for Energy Storage

*Laifa Shen, Qian Che, Hongsen Li, and Xiaogang Zhang**

Binary metal oxides has been regarded as a promising class of electrode materials for high-performance energy storage devices since it offers higher electrochemical activity and higher capacity than mono-metal oxide. Besides, rational design of electrode architectures is an effective solution to further enhance electrochemical performance of energy storage devices. Here, the advanced electrode architectures consisting of carbon textiles uniformally covered by mesoporous $NiCo_2O_4$ nanowire arrays (NWAs) are successfully fabricated by a simple surfactant-assisted hydrothermal method combined with a short post annealing treatment, which can be directly applied as self-supported electrodes for energy storage devices, such as Li-ion batteries, supercapacitors. The as-prepared mesoporous $NiCo_2O_4$ nanowires consist of numerous highly crystalline nanoparticles, leaving a large number of mesopores to alleviate the volume change during the charge/discharge process. Electrode architectures presented here promise fast electron transport by direct connection to the growth substrate and facile ion diffusion path provided by both the abundant mesoporous structure in nanowires and large open spaces between neighboring nanowires, which ensures every nanowire participates in the ultrafast electrochemical reaction. Benefiting from the intrinsic materials and architectures features, the unique binder-free $NiCo_2O_4$/carbon textiles exhibit high specific capacity/capacitance, excellent rate capability, and cycling stability.

1. Introduction

With the increase concerns regarding environmental pollution caused by vast fossil-fuel consumption and the rapid depletion of non-renewable resources,[1] there has been an ever increasing and urgent demand seek renewable and clean energy sources. Energy storage, a key component in energy conversion-storage-delivery chain, has received worldwide concern and increasing research interest.[2–7] Li-ion batteries and supercapacitors are two major devices for electric energy storage. The fast-growing market for portable electronics and the development of hybrid vehicles require further improvement in terms of power and energy density of the energy storage devices. However, carbon is still the dominant electrode material for current Li-ion batteries anodes and commercial supercapacitors, which fails to meet the stringent requirements for future large-scale applications.[8–10]

Transition metal oxides specially Co_3O_4 has been extensively studied as a promising alternative anode materials for Li-ion batteries, offering at least twice the capacity of the most common intercalation anode material, graphite.[11,12] However, due to the fact that cobalt is toxic and expensive, importantly, the low electronic conductivity, serious efforts are made towards replacing Co_3O_4 partially by co-friendly and cheaper alternative metals.[13,14] Recently spinel nickel cobaltice ($NiCo_2O_4$), replacing one cobalt atom by nickel, has been conceived as a promising cost effective and scalable alternative for energy storage owing to its several inherent advantages, including low cost, abundant resources and good environmental benignity.[15–19] More importantly, as a binary metal oxide, the spinel $NiCo_2O_4$ possesses much better electrical conductivity, at least two orders of magnitude higher, and higher electrochemical activity than nickel oxides or cobalt oxides.[20]

Unfortunately, the practical applications of metal oxides are largely hindered due to poor cycling performance and the electrodes cannot maintain their integrity over several discharge–charge cycle. Engineering materials at the nanoscale offers unique electrode properties, such as increased active surface areas, short ion transport pathways, better accommodation of the strains, resulting in enhance the electrochemical energy storage properties of Li-ion batteries and supercapacitors.[21–25] Several different types of $NiCo_2O_4$ nanostructures, including nanoparticles,[26] nanoplatelets,[27,28] nanosheets,[29] nanowires,[30,31] nanotubes,[32] microspheres,[33] the formation of nanocomposites with carbon nanofibers,[34] and graphene,[35] have been recently synthesized and their electrochemical performance is investigated. For example, Lu and co-workers[26] synthesized $NiCo_2O_4$ nanoparticles through an epoxide-assisted sol–gel method and a largely enhanced capacitance is achieved. Yang et al.[36] reported the fabrication of $NiCo_2O_4$/C

L. F. Shen, Q. Che, H. S. Li, Prof. X. G. Zhang
College of Materials Science and Engineering
Key Laboratory for Intelligent Nano Materials and Devices of Ministry of Education
Nanjing University of Aeronautics and Astronautics
Nanjing, 210016, P. R. China
E-mail: azhangxg@nuaa.edu.cn

DOI: 10.1002/adfm.201303138

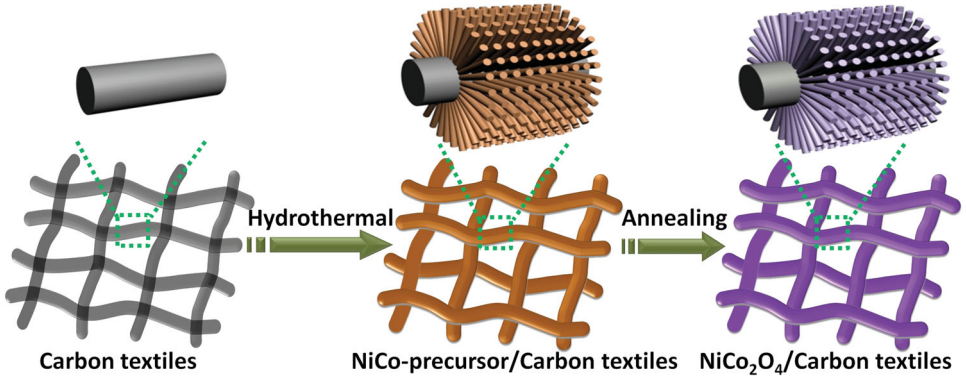

Figure 1. Schematic illustration of the formation of $NiCo_2O_4$ NWAs/carbon textiles composite.

nanocomposite through a hydrothermal method and a high reversible capacity (958.4 mA h g^{-1} under 40 mA g^{-1}) can be achieved. $NiCo_2O_4$ nanostructure materials need to be mixed with polymeric binder and carbon black, and further pressed onto current collector. However, the addition of conductive additive and binder inevitably sacrifices overall energy storage capacity; more importantly, the binder involved will greatly decrease the electrical conductivity of the electrode materials, hindering their potential application in high-performance energy storage devices.[37,38]

Recently, self-supported nanowire arrays (NWAs) growing directly on a current-collecting substrate, such as $Li_4Ti_5O_{12}$ nanowire arrays growing on Ti foil,[39] have been reported to overcome the drawbacks of mixing with conductive carbon and have fast charging/discharging. Mesoporous materials, having high surface areas and abundant pore networks, increase the electrode–electrolyte interfacial area and alleviate the volume change during charge/discharge process.[40,41] Very recently, $NiCo_2O_4$ nanowire grown on metals conductive substrates (nickel foam, Ti foil) have been realized through a simple hydrothermal process.[42,43] However, these self-supported electrode using metals as current collectors exhibits a rigid electrode structures, which makes the devices less flexible, and they also have a low energy density. Recently, many metal oxides electrode materials (e.g., Co_3O_4, MnO_2, NiO, etc.) grown on carbon textiles as self-supported electrode for application in supercapacitors.[13,44–47] Furthermore, the $NiCo_2O_4$ nanowire prepared in the absence of surfactant exhibits a dense suruc-ture and smaller surface areas, which hinders the fast ions mobility and failed to alleviate the volume change during the charge/discharge process, thus drastically decreasing the rate performance and cycling stability. Therefore, it will be of great significance to develop effective methods to grow mesoporous $NiCo_2O_4$ nanowire with abundant porous structure directly on light and flexible substrates for energy storage devices.

In this work, a simple surfactant-assisted hydrothermal method combined with a post annealing treatment is successfully developed to grow mesoporous $NiCo_2O_4$ NWAs on carbon textiles with robust adhesion. Mesoporous $NiCo_2O_4$ nanowires consist of numerous highly crystalline nanoparticles, leaving a large number of mesopores for fast ion transport and alleviating the volume change during the charge/discharge process. The flexible $NiCo_2O_4$/carbon composite textiles can be directly use as a binder-free electrode for Li-ion batteries and supercapacitors, enabling high capacity/capacitance, good cycling stability and excellent rate performance.

2. Results and Discussion

2.1. Morphology and Structural Analysis

The fabrication processes and the resulting novel electrode architectures developed in this work are schematically illustrated in **Figure 1**. Carbon textile (CT) templates were woven by carbon fibers with high flexibility and high conductivity (Figure S1, Supporting Information), making them as unique supporting backbones for controlled growth of mesoporous $NiCo_2O_4$ NWAs for electrochemical energy storage. Firstly, at a proper pH level realized by controlling the mass of urea, well defined NiCo-precursor NWAs can be easily grown on the highly flexible carbon textiles under hydrothermal condition, as described by the following three equations:

$$CO(NH_2)_2 \rightarrow C_3H_6N_6 + 6NH_3 + 3CO_2 \quad (1)$$

$$NH_3 + H_2O \rightarrow NH_4^+ + OH^- \quad (2)$$

$$Ni^{2+} + 2Co^{2+} + 6OH^- \rightarrow NiCo_2(OH)_6 \quad (3)$$

An annealing treatment at 300 °C with a ramping rate of 2 °C min^{-1} is utilized to convert the NiCo-precursor into spinel $NiCo_2O_4$ supported on the carbon textiles, as described by the simple oxidation reaction as follows:

$$NiCo_2(OH)_6 + 1/2O_2 \rightarrow NiCo_2O_4 + 3H_2O \quad (4)$$

The as-synthesized product is first characterized by X-ray diffraction (XRD) to identify its crystallographic structure. As seen from **Figure 2**a, all of the diffraction peaks of the urchin-like $NiCo_2O_4$ microsphere specimen could be indexed to the spinel structure form cubic spinel $NiCo_2O_4$ phase (JCPDS card no. 20-0781). It is generally believed to adopt a spinel-related structure in which nickel occupies the octahedral sites and cobalt is

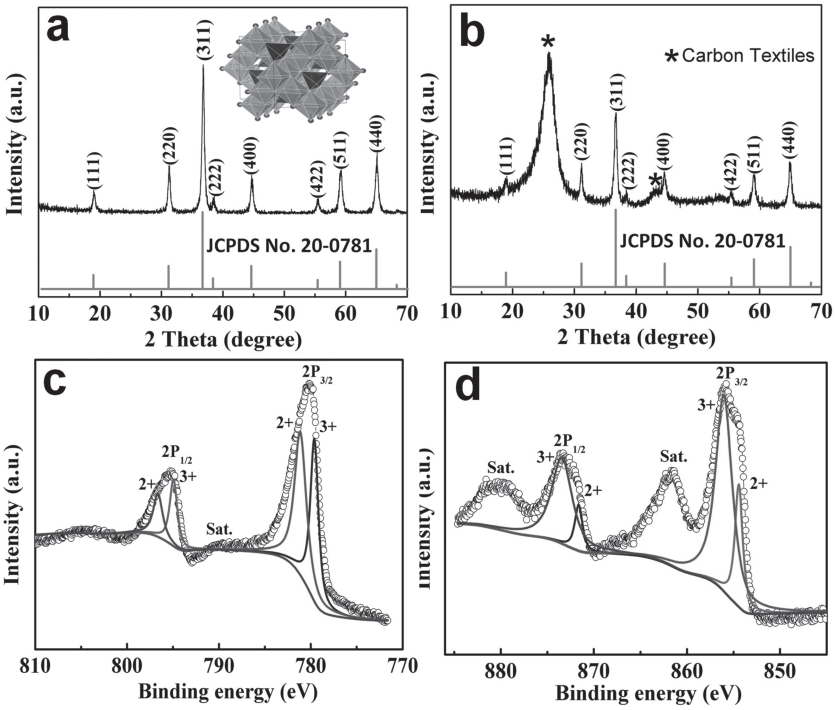

Figure 2. XRD patterns of a) urchin-like $NiCo_2O_4$ microsphere and b) $NiCo_2O_4$ NWAs/carbon textiles composite. High-resolution XPS spectra of c) Co 2p and d) Ni 2p for the $NiCo_2O_4$ naowires scratched down from the carbon textiles.

distributed over both octahedral and tetrahedral sites,[39] as illustrated in the inset of Figure 2a. No residues or contaminants have been detected, indicating the high purity of the sample. The XRD patterns of carbon textiles display a typical graphite (002) and (100) reflection at 26.21° and 43.61°, respectively (Figure S2, Supporting Information). With the exception of the reflections owing to carbon textiles, all peaks in Figure 2b could be indexed to spinel $NiCo_2O_4$ phase. Detailed peak broadening analysis of the (111) XRD reflection using the Scherrer equation indicates that the average crystallite size is approximately 16 nm; this result suggests that the nanowires are composed of nanocrystalline subunits and corroborated by the TEM results. The more detailed elemental composition and oxidation state of the $NiCo_2O_4$ naowires are further characterized by X-ray photoelectron (XPS). The survey spectrum (Figure S3, Supporting Information) indicates the presence of Ni, Co, and O, as well as C from the reference and the absence of other impurities. By using a Gaussian fitting method, the Co 2p emission spectrum (Figure 2c) was best fitted with two spin-orbit doublets, characteristic of Co^{2+} and Co^{3+}, and one shakeup satellite (indicated as "Sat."). The Ni 2p was also fitted with two spin-orbit doublets, characteristic of Ni^{2+} and Ni^{3+}, and two shakeup satellites (Figure 2d). These results show that the chemical composition of mesoporous $NiCo_2O_4$ naowires contain Co^{2+}, Co^{3+}, Ni^{2+}, and Ni^{3+}, which are in good agreement with the results in the literature for $NiCo_2O_4$.[48,49]

The morphology of the different product was examined with scanning electron microscopy (SEM). Figure S4 shows a representative low-magnification SEM image of the NiCo-precursor/CT composite, which clearly displays the well-established texture structure of the NiCo-precursor NWAs grown on the carbon textiles to form a large-scale conformal coating. Higher-magnification SEM images shown in **Figure 3**a,b clearly displays the $NiCo_2O_4$ naowires grown on the carbon microfiber cores to form $NiCo_2O_4$ NWAs/carbon composite fibers. After annealing conversion into spinel $NiCo_2O_4$, the $NiCo_2O_4$ NWAs/carbon textiles composite still keeps the ordered woven structure of the carbon textiles substrate. Inset in Figure 3c shows a digital photograph of $NiCo_2O_4$/carbon textiles electrode that can be folded and flexed, demonstrating the good flexibility. An enlarged view (Figure 3d,e) provides the evidence that the both the nanowire morphology and the array feature of the naowires are perfectly retained after the annealing conversion. This feature could benefit the penetration of the electrolyte, which may contribute to the optimization of electrochemical performance. Typical $NiCo_2O_4$ nanowires have uniform diameters of about 150 nm and length up to several micrometer. In comparison, only $NiCo_2O_4$ nanowire-assembled microsphere will be formed under similar synthesis conditions without the addition of carbon textiles substrates (Figure 3f).

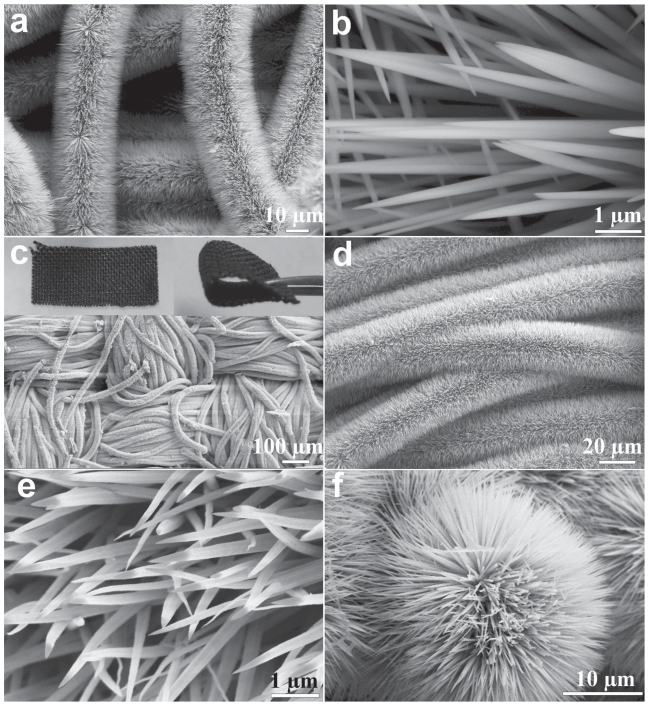

Figure 3. a) Low and b) high magnification SEM images of the NiCo-precursor NWAs/carbon textiles composite, showing all nanowires completely surrounding the carbon microfiber cores. c,d) Low and e) high magnification SEM images of the crystalline $NiCo_2O_4$ NWAs/carbon textiles composite. f) SEM image of the urchin-like $NiCo_2O_4$ microsphere prepared in the absence of carbon textiles.

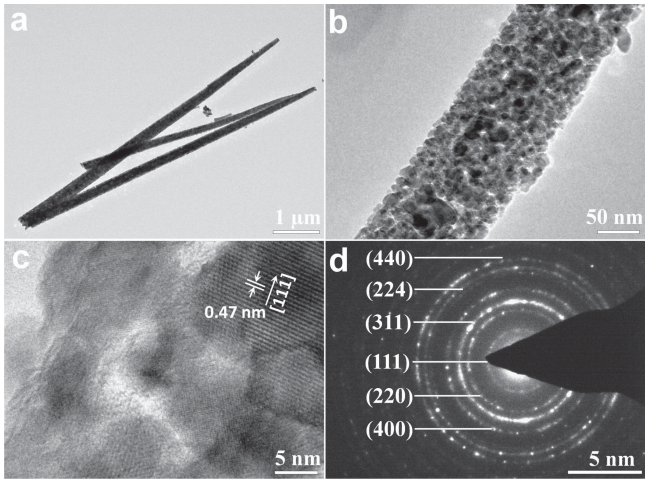

Figure 4. a,b) TEM, c) HRTEM images, and d) SAED pattern of the $NiCo_2O_4$ naowires scratched down from the carbon textiles.

The morphology and structure of $NiCo_2O_4$ nanowires are further elucidated by TEM. As shown in **Figure 4**a, the needle-like $NiCo_2O_4$ nanowires with diameter ≈150 nm and length up to several micrometer can be clearly seen, which are in good agreement with the SEM observation. A higher-magnification TEM image depicted in Figure 4b further reveals that a typical $NiCo_2O_4$ nanowire is actually a porous nanowire composed of many small nanoparticles of 10–20 nm in diameter instead of the conventional single-crystal nanowire. Nitrogen isothermal adsorption-desorption measurements were performed to determine the porosity of the prepared materials. A unimodal peak around 6 nm can be seen in Figure S5 (Supporting Information) for the pore size distribution, which further confirms the mesoporous structure of $NiCo_2O_4$ nanowire. The formation of the mesopores could be related to the gas release during the decomposition of the Ni-Co precursor synthesized using hexamethylenetetramine as capping agent. The mesopores structure enable facile transport of the electrolyte to the surfaces of $NiCo_2O_4$, resulting in rapid charge transfer reactions due to the shorten ions diffusion paths. A lattice spacing of 0.47 nm was observed in Figure 4c, in a good agreement with to the theoretical interplane spacing of spinel $NiCo_2O_4$ (111) planes. The selected-area electron diffraction (SAED) pattern (Figure 4d) shows well-defined diffraction rings, which correspond to the (440), (224), (311), (111), (220), and (400) planes, demonstrating that the sample is polycrystalline with d-spacing consistent with the XRD results (Figure 2b).

2.2. Li-Ion Batteries Performance

Coin-type cell configuration was used to evaluate the lithium storage properties of $NiCo_2O_4$/carbon textiles as a binder-free anode, and the results were compared with $NiCo_2O_4$ microspheres electrode made by the traditional slurry-coating technique. Figure S6 and **Figure 5**a show the charge–discharge profiles of the $NiCo_2O_4$ microspheres electrode and $NiCo_2O_4$/carbon textiles electrode for the first five cycles at a current density of 0.2 A g^{-1} in the range of 0.05 and 3.0 V, respectively. The voltage profile of the first-discharge reaction of $NiCo_2O_4$ comprises mainly two regions, a large plateau at 1 V associated with the irreversible reaction of $NiCo_2O_4$ and Li^+ as Equation 5, which was then followed by a slope till 0.05 V. The first discharge capacity reached about 1317 mA h g^{-1}, equivalent to ≈11.8 mol Li per mole of $NiCo_2O_4$. The voltage profile of the first charge-curve from 0.05–3.0 V does not comprise large plateau regions but only lines of varying slopes. The initial specific charge capacity is about 1018 mA h g^{-1}, corresponding to 77% Coulombic efficiency. Besides the irreversibility of Equation 5, the large irreversible capacity and low Coulombic efficiency for the first cycling is also attributed to the formation of solid electrolyte interface (SEI) film and some undecomposed Li_2O phase.[50]

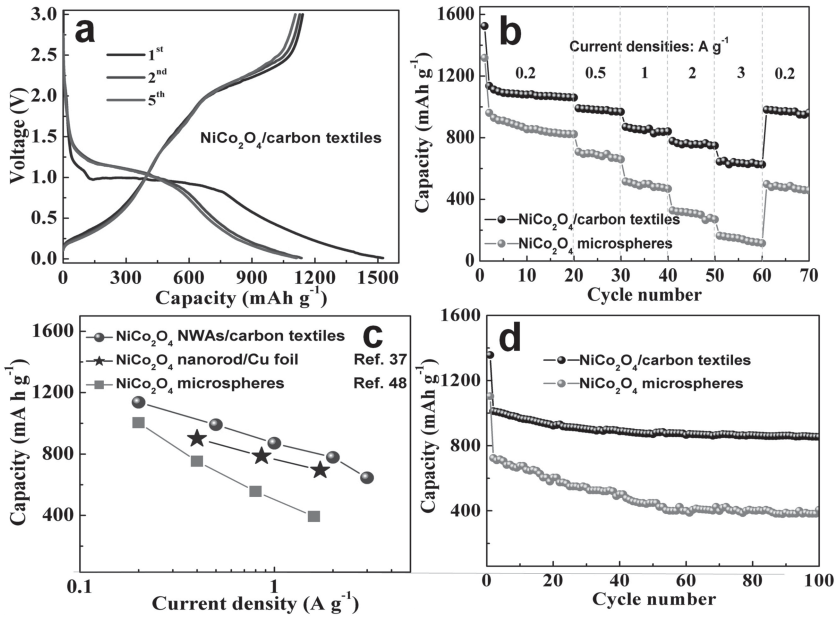

Figure 5. a) Charge–discharge voltage profiles of $NiCo_2O_4$/carbon textiles for the first five cycles at a current density of 0.2 A g^{-1}. b) A comparison of the specific capacity as a function of current density. c) Comparison of rate capability of $NiCo_2O_4$/carbon textiles electrode with other $NiCo_2O_4$ based high-rate electrodes reported recently. d) cycling performance at current densities of 0.5 A g^{-1} of $NiCo_2O_4$/carbon textiles, $NiCo_2O_4$ microspheres.

For the followed discharge process, the potential plateau shifts upward to near 1.1 V with a more sloping profile accompanied by a capacity loss, indicating different electrochemical reactions as Equations 6,7,8. The first discharge capacity of the $NiCo_2O_4$/carbon textiles electrode is around 1524 mA h g^{-1}. The initial Coulombic efficiency is around 76%, and it will quickly increase to 98% after several cycles as shown in Figure 5a. Besides, the carbon textiles exhibit quite low capacity (Figure S7, Supporting Information), indicating that the

carbon textiles makes little contribution to the total specific capacity of the composite electrode.

$$NiCo_2O_4 + 8\,Li^+ + 8e^- = Ni + 2Co + 4Li_2O \quad (5)$$

$$Ni + Li_2O = NiO + 2Li^+ + 2e^- \quad (6)$$

$$2Co + 2Li_2O = 2CoO + 4Li^+ + 4e^- \quad (7)$$

$$2CoO + 2/3Li_2O = 2/3Co_3O_4 + 4/3Li^+ + 4/3e^- \quad (8)$$

The rate performance of $NiCo_2O_4$ microspheres electrode and $NiCo_2O_4$/carbon textiles electrode at various current density were compared in Figure 5b. The $NiCo_2O_4$ microspheres electrode exhibits high initial discharge capacity (1317 mA h g^{-1}), followed however by a sharp capacity decay with the increase of current density. $NiCo_2O_4$/carbon textiles composite electrode, however, exhibited much higher lithium-ion storage capacity and much better rate capability than $NiCo_2O_4$ microsphere electrode. For instance, at a current density 3 A g^{-1}, the capacity of $NiCo_2O_4$/carbon textiles electrode was nearly 4 times greater than $NiCo_2O_4$ microsphere electrode. We also compared this work with other $NiCo_2O_4$ based high-rate electrodes from recent literature,[37,48] and the result shown in Figure 5c. The lithium storage properties of $NiCo_2O_4$ NWAs/carbon textiles is much better than that of $NiCo_2O_4$ nanorod arrays on Cu substrates,[37] $NiCo_2O_4$ microspheres assembled by nanoparticles.[48] For example, the discharge capacity of $NiCo_2O_4$ microspheres assembled by nanoparticles is 1003 mA h g^{-1} at 0.2 A g^{-1},[48] which is close to the discharge capacity of $NiCo_2O_4$ NWAs/carbon textiles. However, the discharge capacity of $NiCo_2O_4$ microspheres decreased steeply with increasing the current density. The capacity (778 mA h g^{-1}) obtained by $NiCo_2O_4$ NWAs/carbon textiles at 2 A g^{-1} is nearly 2 times greater than that obtained at a lower current density of 1.6 A g^{-1} for the $NiCo_2O_4$ microspheres (393 mA h g^{-1}). Moreover, the $NiCo_2O_4$/carbon textiles electrode possesses better cyclic stability than $NiCo_2O_4$ microsphere electrode. Figure 5d shows the discharge capacity as a function of cycle number at current densities of 0.5 A g^{-1} in the voltage range of 0.05–3.0 V. For the $NiCo_2O_4$/carbon textiles electrode, the discharge capacities for the first and second cycles at 0.5 A g^{-1} are 1357 and 1012 mA h g^{-1}, respectively. From the second cycle onwards, the discharge capacity shows only very slow fading. A high discharge capacity of 854 mA h g^{-1} is still achieved after 100 cycles, corresponding to ≈84% of the second discharge capacity. Under the identical test conditions, $NiCo_2O_4$ microsphere electrode exhibit much faster capacity fading, and a capacity of only around 400 mA h g^{-1} is left after 100 cycles at 0.5 A g^{-1}. Compared with those of $NiCo_2O_4$ electrodes reported in literature, the capacity retention of the $NiCo_2O_4$/carbon textiles prepared in this work are better. For example, the capacity of $NiCo_2O_4$ microsphere assembled by nanoparticles can be maintained at 730 mA h g^{-1} after 50 cycles, which is about 67% of the reversible capacity.[48]

The significantly different electrochemical properties for the two electrodes are attributed to the different electrode architectures. Figure S8 (Supporting Information) are the Nyquist plots from AC impedance spectroscopy measurements. These plots clearly show that the diameter of the semicircle of the $NiCo_2O_4$

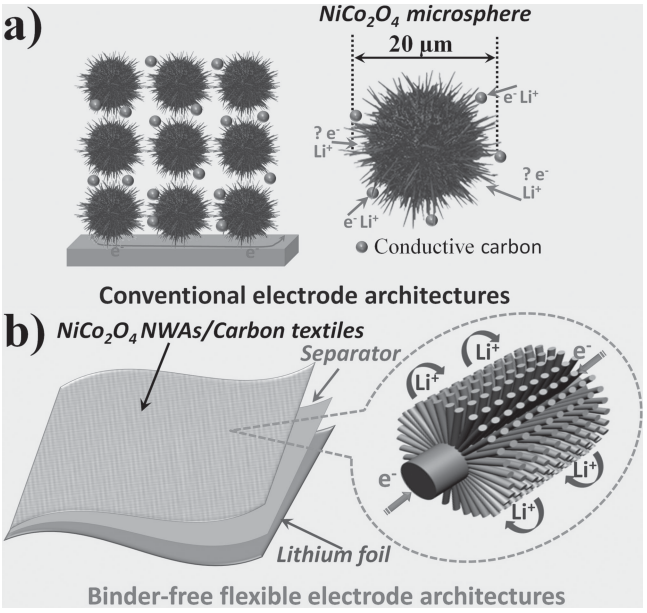

Figure 6. Schematic drawing of a) the conventional $NiCo_2O_4$ microspheres electrode and b) binder-free 3D $NiCo_2O_4$/carbon textiles electrode.

electrode composed of $NiCo_2O_4$ microspheres on Cu foil is much bigger than that of the $NiCo_2O_4$/carbon textiles electrode, indicating that the conventional binder-enriched electrode increase additional undesirable interparticle resistance, more importantly, which failed to provide efficient electron transport between electroactive materials and current collector substrate (**Figure 6**a). The electrochemical reaction pathways is different in our concept of 3D electrode consisting of conductive carbon textiles (current collector) conformal coated with $NiCo_2O_4$ NWAs (Figure 6b): 1) The $NiCo_2O_4$ NWAs directly grown on the carbon textiles with robust adhesion ensure intimate contacts and effective electron transport between the charge collecting substrates of carbon textiles and the every $NiCo_2O_4$ naowires; 2) Loose textures of substrates and large open spaces between neighboring nanowire arrays making more active material exposed to the electrolyte that allow the electrolyte to easily contact with the $NiCo_2O_4$ nanocrystals, providing hierarchical pathways for effective ion transport. 3) Mesoporous $NiCo_2O_4$ nanowire consisting of numerous highly crystalline nanoparticles, leaving a large number of mesopores to accommodate the strain induced by the volume change during the electrochemical reactions and shorten the ion-diffusion length; 4) Additionally, avoiding the use of binders or any conducting additive material in this unique electrode architecture. All of these factors contribute to the effective ambipolar diffusion of ion and e^- into/out of $NiCo_2O_4$ in the $NiCo_2O_4$ NWAs/carbon textiles electrode architecture, enabling remarkable rate capability and good cycling stability.

2.3. Supercapacitors Performance

As another demonstration, the $NiCo_2O_4$/carbon textiles were also used as binder-free electrodes for supercapacitors. The

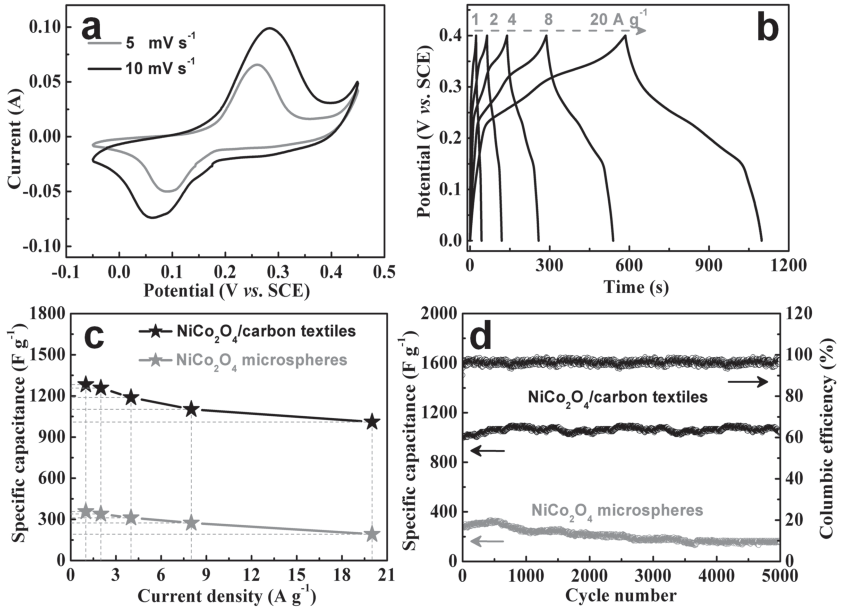

Figure 7. a) CV curves and b) constant-current charge-discharge voltage profiles of $NiCo_2O_4$/carbon textiles. A comparison of the c) specific capacitance as a function of currentdensity, d) cycling performance at current densities of 8 A g^{-1} of $NiCo_2O_4$/carbon textiles, $NiCo_2O_4$ microspheres.

pseudocapacitive properties of the $NiCo_2O_4$/carbon textiles are investigated by cyclic voltammetry (CV) and galvanostatic charge–discharge measurements in three electrode configurations. **Figure 7**a shows the typical CV curves of the $NiCo_2O_4$/carbon textiles electrode at various scan rates ranged from 5 to 10 mV s^{-1}. The shapes of the CV curves clearly confirm the pseudocapacitive behavior, which is distinct from electric double-layer capacitance characterized by nearly rectangular CV curves. Specifically, a pair of well-defined redox peaks can be observed within –0.05 to 0.45 V (vs SCE) is visible in all the CV curves, which is mainly attributed to the Faradaic redox reactions related to M-O/M-O-OH, where M refers to Ni or Co.[18] When increase the scan rate, the peak current increases but the shapes of these CV curves do not significantly change as the scan rate increases from 5 to 10 mV s^{-1}, revealing that this electrode architectures enable fast redox reactions for electrochemical energy storage.

Galvanostatic charge–discharge measurements were conducted at various current densities ranging from 1 to 20 A g^{-1} to further evaluate the pseudocapacitive properties of the as-synthesized self-supported electrode of $NiCo_2O_4$/carbon textiles, and the results are shown in Figure 7b. Evidently, the existence of plateaus at around 0.3 V in the charge-discharge curves suggests the typical pseudocapacitive characteristics, which is in good agreement with the CV curves (Figure 7a). The specific capacitance is calculated by the formula, $C = (I\Delta t)/(m\Delta V)$, where I is the discharge current, Δt is the discharge time, ΔV is the voltage range and m is the mass of the active material. The calculated specific capacitance as a function of the discharge current density is plotted in Figure 7c, and the results were compared with the traditional $NiCo_2O_4$ microsphere electrode. Clearly, the $NiCo_2O_4$/carbon textiles electrode exhibits higher specific capacitance values than binder-enriched $NiCo_2O_4$ microspheres electrode. Specifically, the carbon textiles supported $NiCo_2O_4$ NWAs electrode exhibits excellent pseudocapacitance of 1283, 1258, 1188, 1102, and 1010 F g^{-1} at current densities of 1, 2, 4, 8, and 20 A g^{-1}, respectively. This suggests that about 79% of the SC at 1 A g^{-1} is still retained when the discharge current density is increased to 20 A g^{-1}, which is much higher than that in the previous reports, revealing its good rate capability. However, the specific capacitances of $NiCo_2O_4$ microsphere electrode are only 192 F g^{-1} at 20 A g^{-1}, corresponding to around 54% retention at 1 A g^{-1}.

Supercapacitor are required to operate at high current densities and to have a long cycle life for large scale application. The long-term cycling performances of for two different electrodes are recorded as shown in Figure 7d at a current density of 8 A g^{-1}. Interestingly, the specific capacitance for two electrodes gradually increases during the first 500 cycles, which may attributed to the gradual activation process of the $NiCo_2O_4$ nanoparticles-assembled nanowire. A significantly specific capacitance lose can be seen for $NiCo_2O_4$ microsphere electrode, only 57% of the initial capacitance be maintained after 5000 cycles. While for $NiCo_2O_4$/carbon textiles electrode, the specific capacitance is perfectly retained even after 5000 cycles with a negligible specific capacitance decay demonstrating its superior cyclic stability performance. The Coulombic efficiency (calculated from the discharge–charge capacity) stayed constant at approximately 100%, demonstrating that the perfectly crystalline $NiCo_2O_4$ nanowire supported by carbon textiles form a stable conductive structure on the microscale and that the Faradaic redox reactions is completely reversible even at high current densities. To the best of our knowledge, such remarkable electrochemical stability is rarely observed for $NiCo_2O_4$.[27–30,51]

Based on the above overall electrochemical performance, the unique $NiCo_2O_4$ NWAs/ carbon textiles electrode is apparently superior to many other $NiCo_2O_4$ electrodes except $NiCo_2O_4$ nanosheets supported on Ni foam by Yuan et al. (Mass loading: 0.8 mg cm^{-2}), as can be seen from the Table S1 (Supporting Information). The enormous enhanced specific capacitance and long-term cycling stability of $NiCo_2O_4$/carbon textiles electrode can be attributed to the unique morphology and structure of the electrodes architectures. As the $NiCo_2O_4$ nanowires are composed of nanocrystallites, and possess mesoporosity, the transportation of electrolytes through their nanochannels is possibly more feasible for efficient redox reactions during Faradaic charge storage process. The electronic conductivity of $NiCo_2O_4$/carbon textiles are significantly improved by direct connection to the growth substrate, which ensures every nanowire participates in the ultrafast electrochemical reaction. The above results evidently suggest that it is appealing to use configuration of the $NiCo_2O_4$/carbon textiles as self-supported electrodes for advanced high-performance supercapacitor.

3. Conclusion

In summary, mesoporous $NiCo_2O_4$ NWAs were successfully grown on carbon textiles substrates with robust adhesion through a general surfactant-assisted hydrothermal method and combined with a simple post-annealing treatment. The mesoporous $NiCo_2O_4$ NWAs supported on carbon textiles are directly served as a binder-free electrode for high performance energy storage devices. Electrode design concept presented here allows each $NiCo_2O_4$ nanowire to have its own electrical contact with the carbon fiber substrate and facile ion diffusion path provided by both the abundant mesoporous structure in nanowires and large open spaces between neighboring nanowires, which ensures every nanowire participates in the ultrafast electrochemical reaction. As an anode for Li-ion batteries, the $NiCo_2O_4$/carbon textiles exhibits a reversible capacity of ≈1012 mA h g^{-1} at a current density of 0.5 A g^{-1}, retaining 854 mA h g^{-1} after 100 cycles. A high specific capacitances of 1010 F g^{-1} (79% of the capacitance at 1 A g^{-1}) at 20 A g^{-1} and remarkable cycling stability (No negligible specific capacitance decay after 5000 cycles at 8 A g^{-1}) can be achieved as electrochemical capacitor electrode. More importantly, the electrode design concept can be easily generalized to grown other mesoporous metal oxides nanostructure on substrates for the fabrication of high-performance energy-storage devices.

4. Experimental Section

Growth of $NiCo_2O_4$ NWAs on Carbon Textiles: Carbon textiles was cleaned by ultrasonically in deionized (DI) water, ethanol for 15 min, respectively, and then dried in a oven. In a typical process, 5 mmol $CoCl_2{\cdot}6H_2O$, 2.5 mmol of $NiCl_2{\cdot}6H_2O$, 2 mmol hexadecyl trimethyl ammonium bromide, 9 mmol of urea are dissolved into 50 mL of DI water to form a transparent pink solution. After putting a piece of cleaned carbon cloth (4 cm × 4 cm), the solution was then transferred to a Teflon-lined stainless steel autoclave and kept at 100 °C. After hydrothermal growth, the carbon textiles covered with NiCo-precursor NWAs was carefully rinsed several times with de-ionized water and absolute ethanol with the assistance of ultrasonication, and finally dried in air. Then, the sample was put in a quartz tube and calcined at 300 °C for 3 h to get well defined crystallized $NiCo_2O_4$ NWAs on carbon textiles. In average, 1.2 mg of $NiCo_2O_4$ naowires is grown per 1 cm × 1 cm of carbon textiles, carefully weighted after calcination. $NiCo_2O_4$ naowire-assembled microspheres were also prepared in a similar manner without use of carbon textiles substrate.

Materials Characterization: The crystal structure of the obtained samples was characterized by X-ray diffraction (XRD) (Bruker D8 advance) with Cu Kα radiation. The X-ray photoelectron spectroscopy (XPS) analysis was performed on a Perkin-Elmer PHI 550 spectrometer with Al Kα (1486.6 eV) as the X-ray source. The microstructural properties were characterized using transmission electron microscopy (TEM) (TEM, FEI, Tecnai-20, USA), high-resolution transmission electron microscopy (HRTEM, JEOL JEM-2010), and field-emission scanning electron microscopy (FESEM, JEOL, JSM-7000). The N_2 adsorption–desorption were determined by BET measurements using an ASAP-2010 surface area analyzer.

Electrochemical Measurement: The carbon textiles-supported $NiCo_2O_4$ NWAs directly acted as the working electrode without any ancillary materials. For electrochemical measurements of $NiCo_2O_4$ naowire-assembled microspheres, the working electrode is consisted of active material, carbon black (Super-P-Li), and polymer binder (polyvinylidene fluoride; PVDF) in a weight ratio of 80:10:10. The slurry was pasted to Ni foam (used in supercapacitor) or Cu foil (used in lithium-ion battery) and then dried at 120 °C overnight under vacuum. The supercapacitor tests were conducted with a CHI 660C electrochemical workstation in an aqueous KOH electrolyte (6.0 m) with a three electrode cell where Pt foil serves as the counter electrode and a saturated calomel electrode (SCE) as the reference electrode. Coin cells were assembled in an argon-filled glovebox for a lithium-ion battery. Lithium pellets were used for both the counter and the reference electrodes, and the $NiCo_2O_4$/carbon textiles was directly used as a working electrode. 1 m $LiPF_6$ solution in 1 : 1 (V : V) mixture of ethylene carbonate (EC) and dimethyl carbonate (DMC) was used as electrolyte. The cells were galvanostatically charged and discharged using a Land Battery Tester. Cyclic voltammetry (CV) studies were carried out on an electrochemical workstation (CH Instruments, model 660C). The AC impedance spectrum was measured using a Solatron 1260 impedance analyzer in the frequency range ≈ 10^{-2}–10^6 Hz.

Supporting Information

Supporting Information is available from the Wiley Online Library or from the author.

Acknowledgements

This work was supported by the National Basic Research Program of China (973 Program) (No. 2014CB239701), National Natural Science Foundation of China (No. 21173120, 51372116), Natural Science Foundation of Jiangsu Province (BK2011030).

Received: September 9, 2013
Revised: October 30, 2013
Published online: December 16, 2013

[1] M. Mann, R. Bradley, M. Hughes, *Nature* **1998**, *392*, 779.
[2] B. Dunn, H. Kamath, J. Tarascon, *Science* **2011**, *18*, 928.
[3] Z. Yang, J. Zhang, M. Kintner-Meyer, X. Lu, D. Choi, J. Lemmon, J. Liu, *Chem. Rev.* **2011**, *111*, 3577.
[4] C. Liu, F. Li, L. Ma, H. Cheng, *Adv. Mater.* **2010**, *22*, E28.
[5] L. Shen, H. Li, E. Uchaker, X. Zhang, G. Cao, *Nano Lett.* **2012**, *12*, 5673.
[6] A. Reddy, S. Gowda, M. Shaijumon, P. Ajayan, *Adv. Mater.* **2012**, *24*, 5045.
[7] L. Shen, X. Zhang, E. Uchaker, C. Yuan, G. Cao, *Adv. Energy Mater.* **2012**, *2*, 691.
[8] K. Jost, C. Perez, J. McDonough, V. Presser, M. Heon, G. Dion, Y. Gogotsi, *Energy Environ. Sci.* **2011**, *4*, 5060.
[9] M. Reddy, G. Subba Rao, B. Chowdari, *Chem. Rev.* **2013**, *113*, 5364.
[10] P. Simon, Y. Gogotsi, *Nat. Mater.* **2008**, *7*, 845.
[11] Y. Li, B. Tan, Y. Wu, *Nano Lett.* **2008**, *8*, 265.
[12] Z. Wu, W. Ren, L. Wen, L. Gao, J. Zhao, Z. Chen, G. Zhou, F. Li, H. Cheng, *ACS Nano* **2010**, *4*, 3187.
[13] R. Rakhi, W. Chen, D. Cha, H. Alshareef, *Nano Lett.* **2012**, *12*, 2559.
[14] S. Xiong, C. Yuan, M. Zhang, B. Xi, Y. Qian, *Chem. Eur. J.* **2009**, *15*, 5320.
[15] A. Chadwick, S. Savin, S. Fiddy, R. Alcantara, D. Lisbona, P. Lavela, G. Ortiz, J. Tirado, *J. Phys. Chem. C.* **2007**, *111*, 4636.
[16] R. Alcantara, M. Jaraba, P. Lavela, J. Tirado, *Chem. Mater.* **2002**, *14*, 2847.
[17] A. Thissen, D, Ensling, F. Javier, F. Madrigal, W. Jaegermann, *Chem. Mater.* **2005**, *17*, 5202.
[18] J. Chang, J. Sun, C. Xu, H. Xu, L. Gao, *Nanoscale* **2012**, *4*, 6786.
[19] L. Huang, D. Chen, Y. Ding, S. Feng, Z. Wang, M. Liu, *Nano Lett.* **2013**, *13*, 3135.

[20] C. Yuan, J. Li, L. Hou, X. Zhang, L. Shen, X. Lou, *Adv. Funct. Mater.* **2012**, *22*, 4592.
[21] M. Sassin, C. Chervin, D. Rolison, J. Long, *Acc. Chem. Res.* **2013**, *46*, 1062.
[22] X. Xia, J. Tu, Y. Zhang, X. Wang, C. Gu, X. Zhao, H. Fan, *ACS Nano* **2012**, *6*, 5531.
[23] L. Ji, Z. Lin, M. Alcoutlabi, X. W. Zhang, *Energy Environ. Sci.* **2011**, *4*, 2682.
[24] L. Yuan, X. Lu, X. Xiao, T. Zhai, J. Dai, F. Zhang, B. Hu, X. Wang, L. Gong, J. Chen, C. Hu, Y. Tong, J. Zhou, Z. Wang, *ACS Nano* **2012**, *6*, 656.
[25] M. Wagemaker, F. Mulder, *Acc. Chem. Res.* **2013**, *46*,1206.
[26] T. Wei, C. Chen, H. Chien, S. Lu, C. Hu, *Adv. Mater.* **2010**, *22*, 347.
[27] B. Cui, H. Lin, J. Li, X. Li, J. Yang, J. Tao, *Adv. Funct. Mater.* **2008**, *18*, 1440.
[28] X. H. Lu, X. Huang, S. L. Xie, T. Zhai, C. S. Wang, P. Zhang, M. H. Yu, W. Li, C. L. Liang, Y. X. Tong, *J. Mater. Chem.* **2012**, *22*, 13357.
[29] G. Zhang, X. Lou, *Adv. Mater.* **2013**, *25*, 976.
[30] H. Wang, Q. Gao, L. Jiang, *Small* **2011**, *7*, 2454.
[31] R. Zou, K. Xu, T. Wang, G. He, Q. Liu, X. Liu, Z. Zhang, J. Hu, *J. Mater. Chem. A* **2013**, *1*, 8560.
[32] L. Li, S. Peng, Y. Cheah, P. Teh, J. Wang, G. Wee, Y. Ko, C. Wong, M. Srinivasan, *Chem. Eur. J.* **2013**, *19*, 5892.
[33] Q. Wang, B. Liu, X. Wang, S. Ran, L. Wang, D. Chen, G. Shen, *J. Mater. Chem.* **2012**, *22*, 21647.
[34] G. Zhang, W. X. Lou, *Sci. Rep.* **2013**, DOI: 10.1038/srep01470.
[35] H. Wang, Z. Hu, Y. Chang, Y. Chen, H. Wu, Z. Zhang, Y. Yang, *J. Mater. Chem.* **2011**, *21*, 10504.
[36] Y. Li, P. Zhang, Z. Guo, H. Liu, J. Yang, *Electrochem. Solid-State Lett.* **2008**, *11*, A64.
[37] J. Wang, Y. Zhou, P. Hodgson, Y. Li, *Cryst. Eng. Commun.* **2013**, *15*, 1578.
[38] L. Shen, B. Ding, P. Nie, G. Cao, X. Zhang, *Adv. Energy Mater.* **2013**, *3*, 1484.
[39] L. Shen, E. Uchaker, X. Zhang, G. Cao, *Adv. Mater.* **2012**, *24*, 6502.
[40] Q. Lu, Y. Chen, W. Li, J. Chen, J. Xiao, F. Jiao, *J. Mater. Chem. A* **2013**, *1*, 2331.
[41] Y. Wang, H. Xia, L. Lu, J. Lin, *ACS Nano* **2010**, *4*, 1425.
[42] G. Zhang, H. Wu, H. Hoster, M. Chan-Park, X. Lou, *Energy Environ. Sci.* **2012**, *5*, 9453.
[43] Q. Wang, X. Wang, B. Liu, G. Yu, X. Hou, D. Chen, G. Shen, *J. Mater. Chem. A* **2013**, *1*, 2468.
[44] X. Lu, M. Yu, G. Wang, T. Zhai, S. Xie, Y. Ling, Y. Tong, Y. Li, *Adv. Mater.* **2013**, *25*, 267.
[45] L. Hu, W. Chen, X. Xie, N. Liu, Y. Yang, H. Wu, Y. Yao, M. Pasta, H. N. Alshareef, Y. Cui, *ACS Nano* **2011**, *5*, 8904.
[46] J. Xu, Q. Wang, X. Wang, Q. Xiang, B. Liang, D. Chen, G. Z. Shen, *ACS Nano* **2013**, *7*, 5453.
[47] X. Lu, G. Wang, T. Zhai, M. Yu, S. Xie, Y. Ling, C. Liang, Y. Tong, Y. Li, *Nano Lett.* **2012**, *12*, 5376.
[48] J. Li, S. Xiong, Y. Liu, Z. Ju, Y. Qian, *ACS Appl. Mater. Interfaces* **2013**, *5*, 981.
[49] C. Yuan, J. Li, L. Hou, L. Yang, L. Shen, X. Zhang, *J. Mater. Chem.* **2012**, *22*, 16084.
[50] N. Munichandraiah, L. Scanlon, R. Marsh, *J. Power Sources* **1998**, *72*, 203.
[51] D. Carriazo, J. Patio, M. C. Gutiérrez, M. L. Ferrera, F. Monte, *RSC Adv.* **2013**, *3*, 13690.